Catal Lett (2008) 125:192–196
DOI 10.1007/s10562-008-9593-3

Effect of Mg in Alumina-Supported Sb–V–O Catalysts for the Ammoxidation of Propane into Acrylonitrile

M. Olga Guerrero-Pérez · Jong-San Chang · Do-Young Hong · Jong-Min Lee · Miguel A. Bañares

Received: 25 May 2008 / Accepted: 15 July 2008 / Published online: 13 August 2008

Abstract The effect of Mg as dopant on alumina-supported mixed Sb–V oxide catalysts during the ammoxidation of propane reaction is evaluated. The Mg-doped catalyst increases acrylonitrile selectivity compared to the un-doped Sb–V–O/Al_2O_3 system. The presence of magnesium facilitates the formation of a cationic vacancies enriched rutile $VSbO_4$ phase, involved in C–N triple bond formation. In addition, Mg increases isolation of V^{5+} structural site isolation, which may affect selectivity.

Keywords Sb–V–O/Mg–Al · Sb–V–O/Al · Propane · Ammoxidation · Acrylonitrile

1 Introduction

Acrylonitrile is worldwide used to make acrylic fibres, ABS (acrylonitrile-butadiene-styrene) and SAN (styrene-acrylonitrile) resins, acryl and polyacrylamides, elastomers and other useful products. Nowadays, acrylonitrile is produced by ammoxidation of propylene using promoted Fe–Bi–No–O (bp America) or promoted Fe–Sb–O (Nitto) [1, 2] catalysts, more recently, ammoxidation of renewables would be a new route to acrylonitrile [3]. There has been significant effort towards the direct conversion of propane into acrylonitrile by reaction with ammonia and oxygen as an alternative to the conventional propylene ammoxidation since propylene is more expensive than propane; however, the reaction conditions to activate the C–H bond in propane are more energy demanding, which has a negative effect on selectivity [4, 5]. Several catalytic systems have been studied for this reaction; most promising results are achieved with the Mo–V–Nb system [6–8] and with Sb–V based catalysts [9–11], in particular, the alumina-supported Sb–V catalysts [12, 13].

Sb–V based oxide catalysts are being widely investigated for selective partial oxidation processes. Methanol TPSR profiles show that these materials exhibit highly efficient redox character [14]. They show good performances for the selective oxidation of H_2S to elemental sulfur [15, 16]; for the oxidation of isobutene into methacrolein [17, 18]; for the methane selective oxidation to formaldehyde [19]; for the dehydrogenation of alkylbenzenes with carbon dioxide [20–22] and for the total oxidation of nitrogen-containing organic volatile compounds [23]. They have also been studied for the propane selective oxidation to acrylic acid [24–27] and for the propane ammoxidation to acrylonitrile [28, 29].

Mg–V–Sb bulk oxide catalysts are used during the oxydehydrogenation of alkanes [30–32]. Addition of an appropriate amount of magnesia (Mg/Al = 0.1) to alumina support enhances the stability of Sb–V–O catalysts for the dehydrogenation reaction of ethylbenzene into styrene [33]. This is attributed to the rapid desorption of styrene from MgAl oxide support compared to that of alumina, facilitating desorption of olefins from the catalyst surface which could minimize the carbon accumulation [34, 35]

M. O. Guerrero-Pérez · M. A. Bañares
Instituto de Catálisis y Petroleoquímica (CSIC), Marie Curie, 2, 28049 Madrid, Spain

M. O. Guerrero-Pérez (✉)
Departamento de Ingeniería Química, Facultad de Ciencias, Universidad de Málaga Campus de Teatinos, 29071 Malaga, Spain
e-mail: oguerrero@uma.es; oguerrero@icp.csic.es

J.-S. Chang · D.-Y. Hong · J.-M. Lee
Catalysis Center for Molecular Engineering, Korea Research Institute of Chemical Technology (KRICT), P.O. Box 107, Yuseong, Daejeon 305–600, South Korea

and coke formation. It was demonstrated that a high amount of Mg leads to the formation of magnesium vanadate(s) responsible of a decrease of exposed active V-species and diminishes conversion values [31].

This communication studies the effect on propane ammoxidation to acrylonitrile of doping Mg on alumina-supported Sb–V oxide catalysts. Thus, a sample in which Sb and V oxides were supported over an alumina support modified with an appropriate amount of magnesia (Mg/Al = 0.1) [31] was prepared and characterized. The results were compared with those obtained with a Mg-free sample.

2 Experimental

2.1 Preparation of Samples

MgO-modified alumina (MgAl) supports were obtained by impregnation at room temperature during 2 h of alumina (Aldrich, $S_{BET} = 121\ m^2/g$) with aqueous solutions of $Mg(NO_3)_2 \cdot 6H_2O$ to reach an Mg/Al = 0.1 atomic ratio. The MgAl support was calcined at 670 °C for 4 h in air. Alumina (Al)-or MgAl-supported antimony-vanadium oxide catalysts were prepared by impregnation for 2 h at room temperature with the solutions of NH_4VO_3 and $SbCl_3$ along with tartaric acid; tartaric acid dissolves antimony species completely, thus enabling better entanglement of Sb sites than when the slurry method is used [36]. The catalysts were dried at 120 °C and then calcined at 650 °C for 4 h in air. The loading of the supported Sb–V–O component (20 wt%) was the same for all samples, with an Sb/V atomic ratio of 1.

2.2 Characterization

The catalysts were characterized by nitrogen adsorption, X-ray diffraction (XRD) and Raman spectroscopy. Nitrogen adsorption isotherms were measured at liquid nitrogen temperature with Tristar 3000 model from Micrometrics. Samples were previously degassed at 300 °C for 2 h. Surface area was obtained by BET linearization in the pressure range 0.05–0.2 p/p_0. The average pore sizes were calculated by the BJH method. XRD patterns were recorded with a Miniflex diffractometer from Rigaku using monochromatic Cu Kα radiation. Raman spectra were recorded with a single monochromator Renishaw System 1000 equipped with a cooled CCD detector (−73 °C) and holographic super-Notch filters. The holographic Notch filters remove the elastic scattering while the Raman signal remains high. The samples were excited with the 514 nm Ar line; spectral resolution was ca. 4 cm^{-1} and spectrum acquisition consisted of 20 accumulations of 30 seconds. The spectra were obtained under dehydrated conditions (ca. 120 °C) in a hot stage (Linkam TS-1500). Hydrated samples were obtained at room temperature after and under exposure to a stream of humid synthetic air.

2.3 Activity Measurements

Activity measurements were performed using a conventional microreactor with on-line gas chromatograph equipped with a flame ionization and thermal conductivity detectors. The correctness of the analytical determinations was checked for each test by verification that the carbon balance (based on the propane converted) was within the cumulative mean error of the determinations (±10%). To prevent participation of homogeneous reactivity the reactor was designed with minimum void volume upstream and downstream the catalyst bed. Tests were made using 0.2 g of sample with particle dimensions in the 0.25–0.125 mm range. The axial temperature profile was monitored by a thermocouple sliding inside a tube inserted into the catalyst bed. Catalytic measurements were made using the following feedstock: 25% O_2, 9.8% propane, 8.6% ammonia and helium. The total flow rate was 20 ml/min corresponding to a gas hourly-space velocity (GHSV) of about 3,000 h^{-1}. The amount of catalysts and total flow were determined in order to avoid internal and external diffusion contributions [37]. Yields and selectivities in products were determined on the basis of the moles of propane fed and products obtained, considering the number of carbon atoms in each molecule.

3 Results

Table 1 shows the BET surface area values obtained for both Sb–V samples as well as for bare alumina and Mg-doped alumina. The BET surface area and the pore volume values decrease with Mg addition for both alumina

Table 1 Physicochemical properties of VSb/Al and VSb/MgAl catalysts

Sample	BET surface area (m^2/g)	Pore volume (ml/g)	Average pore size (nm)
Al support	121	0.28	7.9
MgAl support	116	0.26	7.9
VSb/Al	87	0.23	5.2
VSb/MgAl	67	0.20	7.2

and VSb/Al catalyst. It has been shown [31] that the specific surface areas of the catalysts decrease with an increase of Mg content. This effect is attributed to the formation of magnesium vanadate phases; thus, in the present work only a small amount of Mg was added to the catalysts. The average pore size remained similar for both alumina and Mg-modified alumina supports whereas for the catalysts VSb/MgAl showed higher average pore size than VSb/Al.

The XRD patterns are shown in Fig. 1. Both V–SbO/Mg–Al and V–SbO/Al samples showed patterns characteristics of alumina support (JCPDS file 37–1462). Since the patterns for Al_2O_3 and $MgAl_6O_{10}$ phases are almost the same [31], the formation of $MgAl_6O_{10}$ phase in VSb/MgAl catalyst cannot be excluded. Additionally a peak near 27.8° is observed for both samples. Such peak can be associated with the most intense peak of Sb_2O_3 (JCPDS file 11–689) or $VSbO_4$ (JCPDS file 16–0600) patterns. Sb_2O_4 possesses intense Raman bands [12, 38], which are not observed in these samples (Fig. 2); thus, such diffraction pattern must correspond to $VSbO_4$ phase.

Figure 2 shows the Raman spectra of catalysts before and after ammoxidation reaction. There are no Raman bands characteristics of crystalline V_2O_5, Sb_2O_4 or Sb_2O_3 [12]. The Raman band at 1,027 cm^{-1}, sensitive to hydration, is present in all the samples except in the aged VSb/MgAl. This Raman band is characteristic of surface dispersed vanadium oxide species [39]. Fresh VSb/Al sample presents a Raman band near 850 cm^{-1}, which shifts to 800 cm^{-1} in the aged sample. The broad Raman band near 800 cm^{-1} have been assigned to the rutile $VSbO_4$ phase [12]; it appears to be constituted by two Raman bands at 835 and 795 cm^{-1}; these peaks are well resolved with UV Raman spectroscopy [40]. The Raman band near 850 cm^{-1} must present the lineal combination of the Raman band of the stretching mode of bridging oxygen of dispersed polymeric vanadium species [36] near 900 cm^{-1}, with the above described bands of $VSbO_4$. During propane ammoxidation vanadium species tends to disappear and the Raman band near 800 cm^{-1} becomes increasingly

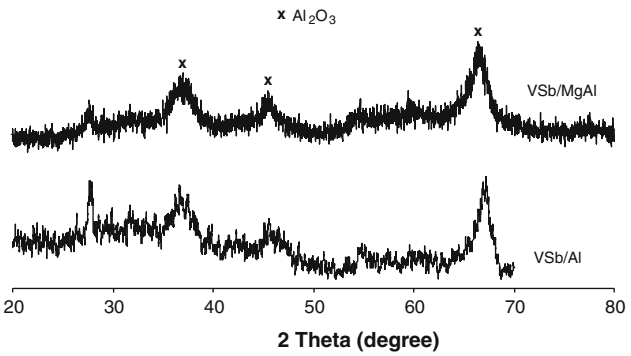

Fig. 1 XRD patterns of VSb/Al and VSb/MgAl samples

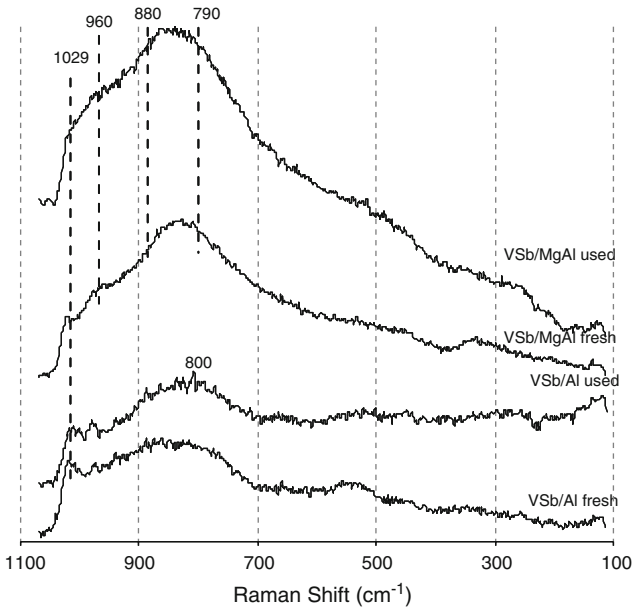

Fig. 2 In situ Raman spectra of fresh and used VSb/Al and VSb/MgAl samples in the dehydrated state

important, this is consistent with previous studies [41–43] with *operando* Raman-GC analyses that showed that activity increases concomitantly to the formation of the rutile $VSbO_4$ phase.

Fresh SbV/MgAl exhibits a broad Raman band near 960 cm^{-1} that has been assigned to pyrovanadate ($Mg_2(V_2O_7)$) [44, 45]. It also possesses a broad feature near 380 cm^{-1} that can be assigned to the bending modes of V–O bonds in magnesium orthovanadate ($Mg_3(VO_4)_2$) [44, 45]. Magnesium orthovanadate presents Raman bands near 825 and 860 cm^{-1}, which must overlap with the broad Raman band of the rutile $VSbO_4$ structure. The presence of V–Mg oxide phases must be very little, since their Raman bands are less intense than those of the rutile $VSbO_4$ phase, which possesses much weaker Raman section [29]. In addition, magnesium orthovanadate Raman bands tend to be sharper and do not overlap. The Raman band of rutile $VSbO_4$ is more intense in Mg-containing samples compared to Mg-free series, thus Mg appears to promote the formation of the rutile $VSbO_4$ phase. It has been described that the differences in the Raman shift of the $VSbO_4$ bands are due to the distortion of the structure due to the interaction of the alumina support with the supported Sb–V–O phase that is related with the number of Sb vacancies at the surface (29). In present paper the interaction with the alumina support is related with the presence of Mg, which appears to promote the formation of these defects.

Both catalysts are stable during time on stream for at least 8 h and the activity results remained stable. Figure 3 shows the propane conversion and selectivity to main products obtained for both catalysts. At 450 °C, both

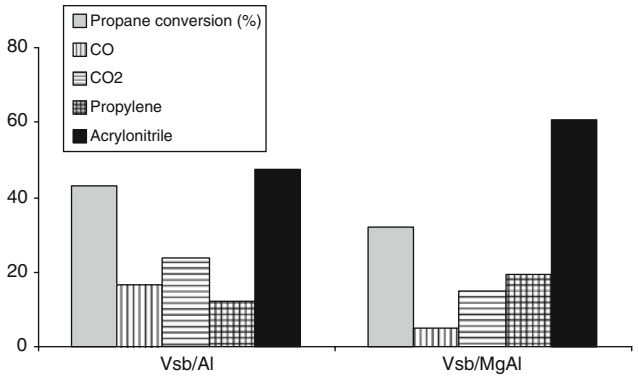

Fig. 3 Catalytic conversion (%) and selectivity during propane ammoxidation on VSb/Al and VSb/MgAl catalysts. Reaction conditions: temperature: 450 °C, total flow 20 ml/min; feed composition (% volume): $C_3H_8/O_2/NH_3/He$ (9.8/25/8.6/56.6), 200 mg of catalysts

samples are selective to acrylonitrile formation. It should be noted that the Mg containing sample affords higher acrylonitrile selectivity due to a lower propane conversion and a lower selectivity to carbon oxides. At higher temperatures (not shown), the VSb/Al sample presents a very high conversion and it is selective to total oxidation compounds whereas VSb/MgAl sample is still selective to acrylonitrile. The Mg-containing catalyst exhibits a broader temperature range in which is selective to acrylonitrile.

4 Discussion

Additives significantly promote ODH activity [46]. The additions of Mg to the alumina-supported V–Sb oxide catalyst clearly promote selectivity to acrylonitrile. Mg-modified catalysts present better results during the dehydrogenation reactions due to olefins from the catalyst surface due to the lower surface acidity [20, 31]. Thus, the production of total oxidation compounds (carbon oxides) decreases Such an effect must promote the chances of propylene to undergo selective ammoxidation to acrylonitrile, which is consistent with the significant increase of acrylonitrile selectivity, and the decrease of COx and propylene production upon addition of Mg. This would account for the higher performance to acrylonitrile.

Figure 2 shows that the broad Raman band of the $VSbO_4$ phase is more intense and shifts to 800 cm^{-1} when Mg is added. This band is described to consist of two bands at 835 and 795 cm^{-1} [40], these Raman bands are related to cation vacancies [43] and underline the highly defective character of the rutile $VSbO_4$ phase. Vanadium antimonates exhibit a continuous non-stoichiometric series [40], with a general formula $Sb_{0.9}V_{0.9+x}O_{0.2-x}O_4$. This facilitates ion mobility in $VSbO_4$-based catalysts [41–43]. The presence of support provides a site for vanadium ions to disperse as surface V^{5+} sites that interact with lattice reduced vanadium sites in the rutile $VSbO_4$ structure, this account for the redox cycle during reaction [41]. Actually, the importance of cation vacancies on the catalytic performance of the rutile structure has been reported before [47–49]. Mg has a high affinity for vanadium; thus, it appears that a higher fraction of vanadium species may detach from the $VSbO_4$ lattice structure due to the interaction of vanadium with Mg species, increasing the amount of vacancies, this would be consistent with the higher intensity of the Raman bands of cation vacancies in the rutile $VSbO_4$ phase (Fig. 2). The presence of such structural changes would account for the better selectivity to acrylonitrile.

Grasselli and co-workers studied the oxydehydrogenation of propane [28, 29] and n-butane [30]. They studied Mg–V based catalysts modified with several metals being Sb the best promoter, which is consistent with our observation on Mg-promoted V–Sb–O catalysts. Those results are related to the high selectivity with the formation of a ternary $Mg_{1-x}SbV_{2/3x}O_{3.5}$ oxide that would contribute to the structural site isolation of the paraffin activating vanadium sites. Our data cannot confirm the formation of ternary $Mg_{1-x}SbV_{2/3x}O_{3.5}$ oxide phases; however, the Raman spectra confirm a more extensive formation of a defective rutile $VSbO_4$ phase, linked to the addition of Mg. Reduced V sites are located into the rutile $VSbO_4$ phase [50, 51], the presence of Mg facilitates cationic (vanadium) vacancies. Dispersed vanadium sites are directly involved in propane activation since Raman bands corresponding to V–OC and VO–C bond vibrations, corresponding to adsorbed alkoxy species on surface V^{5+} species are increasingly important for better performing Sb–V–O catalysts during propane ammoxidation [41]. The redox cycle associated to the ammoxidation of propane is based on the interaction between V^{5+} species dispersed at the surface and reduced V sites in the lattice of $VSbO_4$ [43, 52]. Thus, an enhancement of cation vacancies in the rutile phase would promote the selective ammoxidation of propane to acrylonitrile, which is consistent with its higher selectivity values upon addition of Mg.

5 Conclusions

This work shows that alumina-supported Mg–V–Sb-oxide catalysts are highly promising for the production of acrylonitrile during propane ammoxidation. Mg species contributes to the formation of vanadium cation vacancies in the rutile $VSbO_4$ phase. The stabilization of vanadium cation vacancies would promote an efficient activation for propane ammoxidation to acrylonitrile. In addition, Mg would reduce the number of acidic sites at the catalyst

surface. This would minimize the non-selective oxidation of olefins to CO and CO_2, which in turn, would facilitate N-insertion to form acrylonitrile.

Acknowledgments Spanish Ministry of Education and Science is gratefully acknowledged for financial support (CTQ2005-02802/PPQ). M.O.G.-P. thanks CSIC for an I3PDR-8-02 postdoctoral position. Financial support from KRICT is acknowledged.

References

1. Grasselli RK (1997) In: Ertl G et al (eds) Handbook in catalysis, vol v. Willey-VCH, p 2302
2. Grasselli RK (2003) Top Catal 23:5
3. Guerrero-Pérez MO, Bañares MA (2008) ChemSusChem 1(6):511
4. Bowker M, Bicknell CR, Kerwin P (1996) Appl Catal A 136:205
5. Sokolovskii VD, Davydov AA, Ovsitser O (1995) Catal Rev 37:425
6. Millet JM, Roussel H, Pigamo A, Dubois JL, Jumas JC (2002) App Catal A: Gen 232:77
7. Vaarkamp M, Ushikubo T (1998) App Catal A: Gen 174:99–107
8. Guerrero-Pérez MO, Al-Saeedi JN, Guliants VV, Bañares MA (2004) App Catal A 260:93
9. Andersson A, Andersson SLT, Centi G, Grasselli RK, Sanati M, Trifiro F (1993) Stud Surf Sci Catal 75:691
10. Nilsson J, Landa Canovas A, Hansen S, Andersson A (1997) Catal Today 33:97
11. Guerrero-Pérez MO, Martínez-Huerta MV, Fierro JLG, Bañares MA (2006) App Catal A 298:1
12. Nilsson J, Landa Canovas AR, Hansen S, Andersson A (1996) J Catal 160:244
13. Guerrero-Pérez MO, Fierro JLG, Vicente MA, Bañares MA (2002) J Catal 206:339
14. Guerrero-Pérez MO, Kim TJ, Bañares MA, Wachs IE (2008) J Phys Chem C (submitted)
15. Park DW, Park BK, Park DK, Woo HC (2002) Appl Catal A 223:215
16. Kim BG, Park DW, Kim I, Woo HC (2003) Catal Today 87:11
17. Shishido T, Inoue A, Konishi T, Matsuura I, Takehira K (2000) Catal Lett 68:215
18. Guan J, Jia M, Ping J, Wang Z, Xing L, Xu H, Kan Q (2006) Catal Lett 108:125
19. Zhang H, Zhang J, Sun K, Feng Z, Ying P, Li L (2006) Catal Lett 106:89
20. Chang J-S, Vislovskiy VP, Park SE, Hong D-Y, Yoo JS, Park S-E (2003) Green Chem 5:87
21. Vislovski VP, Chang J-S, Park M-S, Park S-E (2003) Catal Commun 3:227
22. Park M-S, Vislovskiy VP, Chang J-S, Shul Y-G, Yoo JS, Park S-E (2003) Catal Today 87:205
23. Guerrero-Pérez MO, Janas J, Machej T, Haber J, Lewandowska AE, Bañares MA (2007) App Catal B 71:85
24. Blasco T, Botella P, Concepción P, López Nieto JM, Martínez-Arias A, Prieto C (2004) J Catal 228:362
25. Al-Saeedi JN, Guliants VV, Guerrero-Pérez MO, Bañares MA (2003) J Catal 215:108
26. Guliants VV, Bhandari R, Al-Saeedi JN, Vasudevan VK, Soman R, Guerrero-Pérez O, Bañares MA (2004) Appl Catal A 274:123
27. Ueda W, Endo Y, Watanabe N (2006) Top Catal 38:261
28. Centi G, Perathoner S, Trifirô F (1997) Appl Catal A 157:143
29. Guerrero-Pérez MO, Vicente MA, Fierro JLG, Bañares MA (2007) Chem Matter 19:6621
30. Michaels JN, Stern DL, Grasselli RK (1996) Catal Lett 42:135
31. Michaels JN, Stern DL, Grasselli RK (1996) Catal Lett 42:139
32. Stern DL, Michaels JN, DeCaul L, Grasselli RK (1997) Appl Catal A 153:21
33. Hong D-Y, Chang J-S, Vislovskiy VP, Park S-E, Yoo JS (2006) Chem Lett 35:2
34. Machli M, Heracleous E, Lemonidou AA (2002) Appl Catal 236:23
35. Evans OR, Bell AT, Tilley TD (2004) J Catal 226:292
36. Guerrero-Pérez MO, Fierro JLG, Bañares MA (2006) Top Catal 41:43
37. Guerrero-Pérez MO, PhD Dissertation (2003) Universidad Autónoma de Madrid, Spain
38. Guerrero-Pérez MO, Fierro JLG, Bañares MA (2003) Catal Today 78:387
39. Bañares MA, Wachs IE (2002) J Raman Spectrosc 33:359
40. Xiong G, Sullivan VS, Stair PC, Zajac GW, Trail SS, Kaduk JA, Golab JT, Brazdil JF (2005) J Catal 230:317
41. Guerrero-Pérez MO, Bañares MA (2002) Chem Commun 12:1292
42. Bañares MA, Guerrero-Pérez MO, Fierro JLG, Córtez GG (2002) J Mater Chem 12:3337
43. Guerrero-Pérez MO, Bañares MA (2007) J Phys Chem C 111:1315
44. Pless JD, Bardin BB, Kim H-S, Ko D, Smith MT, Hammond RR, Stair PC, Poeppelmeier KR (2004) J Catal 223:419
45. Vidal-Michel R, Hohn KL (2004) J Catal 221:127
46. Samson K, Grzybowska B (2007) Polish J Chem 81:1345
47. Ballarini N, Cavani F, Cimini M, Trifirò F, Mollet JMM, Cornaro U, Catani R (2006) J Catal 241:255
48. Cimini M, Millet JMM, Cavani F (2004) J Solid State Chem 177:1045
49. Roussel H, Mehlomakulu B, Belhadj F, van Steen E, Millet JMM (2007) J Catal 205:97
50. Berry FJ, Brett ME, Patterson J (1983) J Chem Soc Dalton Trans 9
51. Birchall T, Sleight AW (1976) Inorg Chem 15:868
52. Guerrero-Pérez MO, Bañares MA (2004) Catal Today 96:265